Phys. Status Solidi B **246**, No. 4, 766–770 (2009) / **DOI** 10.1002/pssb.200880581

physica status solidi b
www.pss-b.com
basic solid state physics

# Magnetic and structural properties of transition metal doped zinc-oxide nanostructures

**Amélia O. Ankiewicz[*, 1], Wolfgang Gehlhoff[2], Joana S. Martins[1], Ângela S. Pereira[3], Sérgio Pereira[3], Axel Hoffmann[2], Evgeni M. Kaidashev[4], Andreas Rahm[4], Michael Lorenz[4], Marius Grundmann[4], Maria C. Carmo[1], Tito Trindade[3], and Nikolai A. Sobolev[1]**

[1] I3N and Departamento de Física, Universidade de Aveiro, Campus de Santiago, 3810-193 Aveiro, Portugal
[2] Institut für Festkörperphysik, Technische Universität Berlin, 10623 Berlin, Germany
[3] CICECO, Universidade de Aveiro, Campus de Santiago, 3810-193 Aveiro, Portugal
[4] Institut für Experimentelle Physik II, Universität Leipzig, 04103 Leipzig, Germany

Received 21 April 2008, revised 5 October 2008, accepted 28 October 2008
Published online 22 January 2009

**PACS** 61.72.Vv, 68.65.La, 75.50.Pp, 76.30.Fc, 81.07.Bc

[*] Corresponding author: e-mail amelia@ua.pt, Phone: +351 234 378 106, Fax: +351 234 378 197

We report on the magnetic and structural properties of two types of nanostructures doped with Co or Mn, namely, ZnO nanowires and colloidal ZnO nanocrystals. Electron paramagnetic resonance (EPR) spectra have been measured and analysed to extract information on the incorporation of the ions in the lattice. A detailed analysis by means of simulations of the experimental EPR spectra confirms that the transition metal (TM) ions were mainly incorporated as $TM^{2+}$, occupying the $Zn^{2+}$ sites in the wurtzite structure of ZnO. Furthermore, for both types of nanostructures, the EPR spectra are composed of more than one signal, revealing locally distorted environments or core-shell structures, proved by surface modifications via inorganic coatings.



**1 Introduction** Several research groups all over the world have been intensively studying transition metal (TM) doped ZnO [1, 2], since it has been predicted to be one of the most promising candidates for a wide band gap diluted magnetic semiconductor (DMS) [3–5]. The diversity of results [6–12] has set a heated dispute about the existence of ZnO based DMSs and the nature of magnetism observed in this material.

Electron paramagnetic resonance (EPR) spectroscopy is a powerful technique for probing the microscopic environment of transition metal ions in semiconductors. In the present work, we employed EPR to study two types of ZnO nanostructures doped with Co or Mn during growth, namely, ZnO nanowires (NWs) and colloidal ZnO nanocrystals (NCs). Structural characterization was carried out by means of X-ray diffraction (XRD), scanning electron microscopy (SEM) and transmission electron microscopy (TEM).

**2 Sample preparation** The ZnO NWs samples were synthesized on *a*-plane sapphire substrates by high-pressure PLD [13, 14]. The PLD targets of the three NWs samples, NW1, NW2 and NW3, were prepared from pressed and sintered 5N powders nominally containing 3 at% Mn, 10 at% Mn or 5 at% Co, respectively. The details of the growth process have been published elsewhere [14].

The ZnO colloidal NCs were synthesized through a method reported by Norberg et al. [6]. Mn or Co doping was achieved by addition of $TM(CH_3COO)_2 \cdot H_2O$ (TM = Mn, Co) to the $Zn(CH_3COO)_2 \cdot 2H_2O$ precursor solution. Samples nominally doped with 5 at% Mn (sample NC1), 10 at% Mn (sample NC2) or 5 at% Co (sample NC3) were prepared. Part of the original ZnO:Co NCs were subjected to chemical surface modification, either by encapsulation with polystyrene (PS) (sample NC4) or by forming ZnSe shells at the surface of the NCs (sample NC5), by means of a reaction with TOPSe and at the expense of the ZnO, as explained in detail in Ref. [15].

**3 Structural characterization** Elemental analysis of samples NW1 and NW3 was carried out by Rutherford

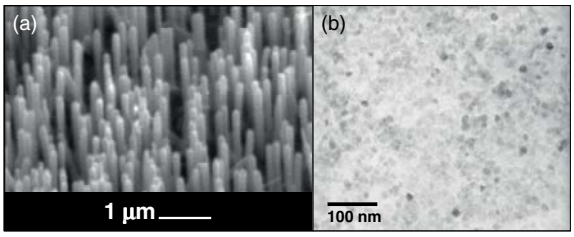


**Figure 1** (a) Typical SEM image of the ZnO nanowires, taken under 45° viewing angle for the nominally 3 at% Mn doped ZnO NWs. (b) Typical TEM image of the ZnO colloidal nanocrystals, taken for the 5 at% doped Mn ZnO NCs.

Backscattering (RBS) in a previous work [14]. For the first sample the Mn content varied between 0.20 at% and 0.75 at%, while for the second one the Co content varied between 0.15 at% and 0.3 at%. In both cases, the RBS measurements show that the doping content in the NWs is much lower than that expected from the target compositions. A typical SEM picture of the studied NWs is given in Fig. 1(a), evidencing the alignment perpendicular to the substrate surface. The structures are about 1 µm long, have a hexagonal cross-section and diameters ranging from 60 nm to 150 nm.

In Fig. 1(b) we show a typical TEM image of the studied ZnO NCs, which are morphologically well-defined particles with an approximately spherical shape. The results of the XRD measurements for the ZnO NCs plotted in Fig. 2 evidence the formation of ZnO NCs with a hexagonal

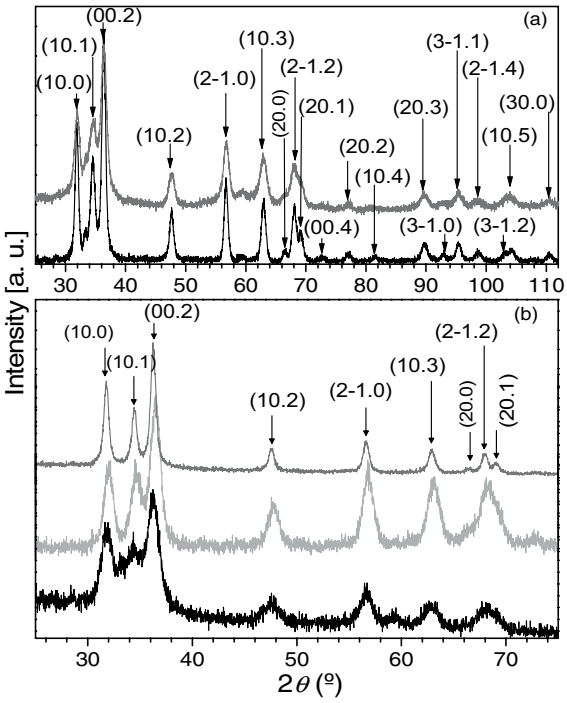


**Figure 2** XRD measurements of (a) ZnO NCs doped with 5% Mn (NC1, black trace) and 10% Mn (NC2, dark gray); (b) ZnO NCs doped with 5% Co (NC3, black), polystyrene capped (NC4, light gray) or ZnSe capped (NC5, dark gray) ZnO : 5% Co NCs.

wurtzite crystal structure. No TM clusters or TM-related complexes were detected, at least within the sensitivity of the apparatus. Excluding instrument-related broadening effects (using a certified standard NIST SRM660a (LaB6 powder)) and applying the Scherrer equation, we estimate the crystallite size as a function of the peak width, yielding average diameters of 13 ± 0.5 nm, 8.2 ± 0.5 nm, 6 ± 2 nm, 6 ± 2 nm and 12 ± 3 nm for the ZnO NCs in samples NC1, NC2, NC3, NC4 and NC5, respectively.

**4 EPR results and discussion** EPR measurements were performed in the X band (~9.5 GHz) for all ZnO samples, at temperatures between 4 K and 300 K, using a Bruker ESP 300E spectrometer equipped with an Oxford Instruments continuous flow helium cryostat.

As with all 3d TM ions, Mn and Co are expected to substitute the Zn ions having a $C_{3v}$ point symmetry in the ZnO wurtzite structure.

**4.1 Mn incorporation** From the measured EPR spectra, the Mn is substitutional on Zn sites yielding a $3d^5$ electron valence configuration and a $^6A_1$ ground state, with a nuclear spin $I = 5/2$ and an electron spin $S = 5/2$. The EPR data is thus described by the spin Hamiltonian (SH) given by [16]:

$$\begin{aligned}\hat{H}_S = {} & \mu_B \boldsymbol{B}\cdot g\cdot \boldsymbol{S} + \boldsymbol{S}\cdot A\cdot \boldsymbol{I} + D\left[S_Z^2 - \frac{35}{12}\right] \\ & - \frac{(a-F)}{180}\left[35S_Z^4 - \frac{475}{2}S_Z^2 + \frac{2835}{16}\right] \\ & + \frac{a\sqrt{2}}{36}\left[S_Z(S_+^3 - S_-^3) + (S_+^3 - S_-^3)S_Z\right], \end{aligned} \quad (1)$$

with $S_\pm = S_X \pm iS_Y$, where $\mu_B$ is the Bohr magneton, $B$ is the applied magnetic field, $g$ and $A$ are the $g$-tensor and the hyperfine (HF) tensor, respectively, $D$ and $F$ are the axial fine structure (FS) parameters given by the spin operators in second and fourth order, respectively, and $a$ is the cubic FS parameter. The crystal $c$-axis (cubic [111] axis) was chosen as the quantization axis $Z$, with $X$ and $Y$ being, in cubic notation, $[11\bar{2}]$ and $[\bar{1}10]$ axis, respectively. We will refer to the symbols ∥ and ⊥ to designate the applied magnetic field parallel and perpendicular to the $c$-axis, respectively.

For the NWs, the angular dependence of the spectrum yields full information needed for the determination of the SH parameters, and one can use perturbation theory to obtain analytical solutions in special directions [9]. For both Mn contents, we find that the signal stems from the substitutional Mn. With increasing Mn content, the linewidth increases due to the dipole–dipole interaction of the paramagnetic ions. For the nominal $x_{Mn} = 10$ at%, an additional broad line appears, probably stemming from regions with higher spin concentrations, where the HF structure of the spectra is obscured by the dipole–dipole broadening and breaks down due to the exchange interaction.

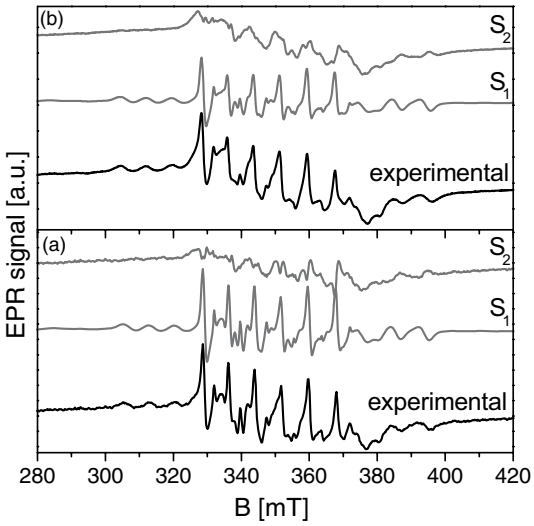


**Figure 3** EPR spectrum of (a) 5% and (b) 10% Mn doped colloidal ZnO NCs, measured at 295 K, along with the respective simulations of substitutional $Mn^{2+}$ on Zn sites ($S_1$) and $S_2$ being the difference between the experimental spectrum and $S_1$.

In the case of powder spectra as shown in Fig. 3, one has to fully integrate over the space angles in order to calculate the SH parameters. For the NCs we performed exact diagonalization of the SH given in Eq. (1) and simulated the respective spectra using the EasySpin software package [17]. The determined SH parameters for both Mn-doped ZnO nanostructures are given in Table 1.

For the NCs, the simulations reveal that the EPR spectrum is composed by two signals: $S_1$ being due to substitutional $Mn^{2+}$ in the core of the NCs, described by the usual SH parameters, and $S_2$, with larger $A$-values (~9 mT), given by the difference between the experimental signal and $S_1$. For Mn in NCs the strain is larger than in bulk crystals, due to the larger surface-to-volume ratio in the former, and we found it necessary to introduce a Gaussian distribution of the $D$-values with $\Delta D = 4$ mT in order to simulate the substitutional $Mn^{2+}$ in the core. Signal $S_2$ is composed by six lines that are the fingerprint of Mn ($I = 5/2$). The apparently larger HF splitting might be related to the increase of the bond ionicity [19] due to functionalization of the surface. Additionally, with increasing Mn content the particle size decreases, and consequently the surface-to-volume ratio increases, as well as the relative intensity of $S_2$. These facts allow us to ascribe $S_2$ to Mn in the surface shell of the NCs, in agreement with the empirical results of Ref. [6].

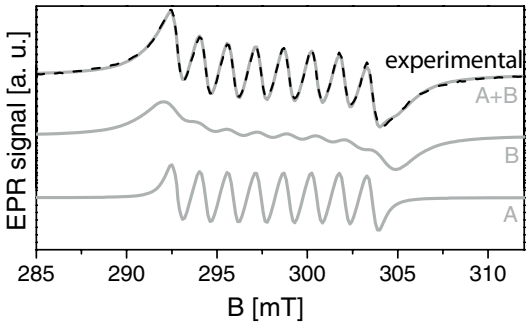


**Figure 4** Experimental EPR spectrum (black) of $Co^{2+}$ in ZnO NWs (sample NW3), measured at 4.2 K for $B \parallel c$ ($\theta = 0°$), superimposed with the result of the fitting given by the sum of components A and B (light gray).

**4.2 Co incorporation** In the case of substitutional $Co^{2+}$ ($3d^7$) on the Zn sites the ground state is the $^4A_2$ orbital singlet. Due to the strong hexagonal crystal field, the zero-field splitting is much larger than the Zeeman energy, hence only the electron spin transitions within the $|\pm 1/2\rangle$ doublet can be observed in the available magnetic field range. Thus, we can describe the spectra within a good approach by the formalism of the effective SH [9]:

$$\hat{H}_S = \mu_B \boldsymbol{B} \cdot g' \cdot \boldsymbol{S}' + \boldsymbol{S}' \cdot A' \cdot \boldsymbol{I}\,, \tag{2}$$

where all symbols have their usual meanings, the prime indicates the effective values, and $I = 7/2$ and $S' = 1/2$.

In the case of the Co doped NWs, as shown in Fig. 4, the EPR spectrum consists of two paramagnetic signals A and B with different linewidths, whose relative intensities give the concentration ratio of the respective paramag-

**Table 1** Spin Hamiltonian parameters for substitutional $Mn^{2+}$ on Zn sites, in Mn doped ZnO nanostructures. Except for the $g$-values, all values are given in $10^{-4}$ cm$^{-1}$.

| | nanowires | | nanocrystals | | bulk |
|---|---|---|---|---|---|
| $x_{Mn}$ | 3 at% | 10 at% | 5 at% | 10 at% | Ref. [18] |
| $g_\parallel$ | 2.003 ±0.001 | 2.000 ±0.002 | 2.001 ±0.001 | 2.002 ±0.001 | 2.0012 ±0.0002 |
| $g_\perp$ | – | – | 2.001 ±0.001 | 2.002 ±0.001 | |
| $A_\parallel$ | −76 ± 1 | −78 ± 3 | −73.9 ± 0.5 | −73.9 ± 0.5 | −74.10 ± 0.05 |
| $A_\perp$ | – | – | −73.5 ± 0.5 | −73.0 ± 0.5 | |
| $D$ | −231 ± 1 | −230 ± 3 | −231 ± 5 | −236 ± 5 | −236.2 ± 0.4 |
| $(a-F)$ | 6 ± 1 | 7 ± 3 | 5.23 | 5.23 | 5.23 ± 0.05 |

 

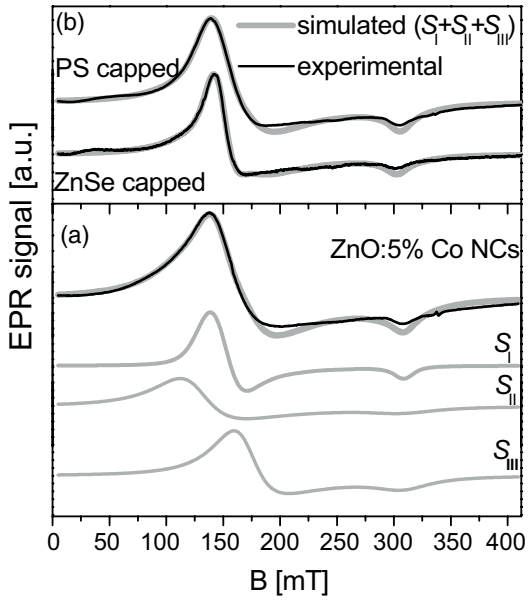


**Figure 5** Experimental EPR spectra (black) measured at 10 K for (a) raw 5% Co doped ZnO NCs (sample NC3) and (b) those capped with polystyrene (PS) (sample NC4) or ZnSe (sample NC5), superimposed with the result of the respective simulation (light gray) given by the sum of the components $S_I$, $S_{II}$ and $S_{III}$.

netic centres $N_B/N_A = 1.4$. Both components yield SH parameters ($g'_{\|} = 2.25$, $g'_{\perp} = 4.56$, $A'_{\|} = 16.2 \times 10^{-4}$ cm$^{-1}$, and $A'_{\perp} = 3.2 \times 10^{-4}$ cm$^{-1}$) in agreement with those of substitutional $Co^{2+}$ on Zn sites [20], follow the same angular and temperature dependencies, and so probably stem from two different $Co^{2+}$ environments, which may be due to different local concentration of Co ions and/or different local strains.

In the case of the Co doped ZnO NCs, the EPR powder spectra have been simulated by diagonalization of the SH given in Eq. (2) and full integration over the space angles using EasySpin [17]. The analysis shows that the spectra are composed by three distinct signals: $S_I$ due to substitutional $Co^{2+}$ in the core of the NCs with effective SH parameters $g'_{\|} = 2.2$, $g'_{\perp} = 4.6$, $A'_{\|} = 16.0 \times 10^{-4}$ cm$^{-1}$, and $A'_{\perp} = 3.0 \times 10^{-4}$ cm$^{-1}$, in agreement with the bulk values [20]; $S_{II}$ and $S_{III}$, probably caused by locally distorted environments and described by $g'_{\|} = 2.2$, $g'_{\perp} = 5.3$, and $g'_{\|} = 2.2$, $g'_{\perp} = 3.9$ for $S_{II}$ and $S_{III}$, respectively. Representatively, the simulations of the three EPR signals for sample NC3 are shown in Fig. 5(a), along with the final result of the simulations of the EPR spectra for the surface modified samples given in Fig. 5(b), with the respective experimental traces. The surface exchange reaction with TOPSe occurring during the preparation of sample NC5, in which ZnSe is formed at the expense of ZnO in the shell of the NCs, partially removes the $S_{II}$ and $S_{III}$ signals, revealing a core-shell structure. As expected, this effect is not so pronounced for sample NC4, as the surface is not removed by the PS encapsulation.

**5 Summary and conclusion** Mn or Co ions were successfully incorporated both into ZnO NWs and NCs, yielding the EPR spectra of isolated $Mn^{2+}$ or $Co^{2+}$, respectively, on Zn sites. No evidence of ferromagnetism was found in any case. For both types of nanostructures, the TM incorporation was heterogeneous in the sense that the EPR spectra were always composed partly of a signal stemming from substitutional TM ions on Zn sites, and partly of that coming from TM ions in distorted or TM enriched environments. Furthermore, we have proved that the TM doped colloidal ZnO NCs exhibit a core-shell structure revealed by the relative intensities of the EPR spectra and by the performed surface modifications. Our experiments show that the EPR analysis allows us to directly demonstrate whether and where the TM ions are incorporated and evidence the importance of the surface effects at material dimensions below ~15 nm, which where not observed for the larger structures.

**Acknowledgements** This work was supported by FCT (Project PTDS/FIS/72843/2006, grant SFRH/BD/21569/2005) and SANDiE Network of Excellence.

## References

[1] C. Liu, F. Yun, and H. Morkoç, J. Mater. Sci., Mater. Electron. **16**, 555 (2005), and references therein.
[2] T. Dietl, J. Appl. Phys. **103**, 07D111 (2008), and references therein.
[3] T. Dietl, H. Ohno, M. Matsukura, J. Cibert, and D. Ferrand, Science **287**, 1019 (2000).
[4] K. Sato and H. Katayama-Yoshida, Jpn. J. Appl. Phys., Part 2 **39**, L555 (2000).
[5] H. Katayama-Yoshida, K. Sato, and T. Yamamoto, JSAP Int. **6**, 20 (2002).
[6] N. S. Norberg, K. R. Kittilstved, J. E. Amonette, R. K. Kukkadapu, D. A. Schwartz, and D. R. Gamelin, J. Am. Chem. Soc. **126**, 9387 (2004).
[7] P. Sharma, A. Gupta, K. V. Rao, F. J. Owens, R. Sharma, R. Ahuja, J. M. Osorio Guillen, B. Johansson, and G. A. Gehring, Nature Mater. **2**, 673 (2003).
[8] K. Ueda, H. Tabat, and T. Kawai, Appl. Phys. Lett. **79**, 988 (2001).
[9] A. O. Ankiewicz, W. Gehlhoff, E. M. Kaidashev, A. Rahm, M. Lorenz, M. Grundmann, M. C. Carmo, and N. A. Sobolev, J. Appl. Phys. **101**, 024324 (2007).
[10] M. H. Kane, K. Shalini, C. J. Summers, R. Varatharajan, J. Nause, C. R. Vestal, Z. J. Zhang, and I. T. Ferguson, J. Appl. Phys. **97**, 023906 (2005).
[11] M. Diaconu, H. Schmidt, A. Pöppl, R. Böttcher, J. Hoentsch, A. Rahm, H. Hochmuth, M. Lorenz, and M. Grundmann, Superlattices Microstruct. **38**, 413 (2005).
[12] N. Volbers, H. Zhou, C. Knies, D. Pfisterer, J. Sann, D. M. Hofmann, and B. K. Meyer, Appl. Phys. A, Mater. Sci. Process. **88**, 153 (2007).
[13] M. Lorenz, E. M. Kaidashev, A. Rahm, Th. Nobis, J. Lenzner, G. Wagner, D. Spemann, H. Hochmuth, and M. Grundmann, Appl. Phys. Lett. **86**, 143113 (2005).

[14] A. Rahm, E. M. Kaidashev, H. Schmidt, M. Diaconu, A. Pöppl, R. Böttcher, C. Meinecke, T. Butz, M. Lorenz, and M. Grundmann, Microchim. Acta **156**, 21 (2006).
[15] A. S. Pereira, A. O. Ankiewicz, W. Gehlhoff, A. Hoffmann, S. Pereira, T. Trindade, M. Grundmann, M. C. Carmo, and N. A. Sobolev, J. Appl. Phys. **103**, 07D140 (2008).
[16] J. Kreissl, K. Irmscher, W. Gehlhoff, P. Omling, and P. Emanuelsson, Phys. Rev. B **44**, 3678 (1991) and references therein.
[17] S. Stoll and A. Schweiger, J. Magn. Reson. **178**, 42 (2006).
[18] J. Schneider, S. R. Sircar, and A. Räuber, Z. Nat.forsch. **18a**, 980 (1963); Z. Nat.forsch. **17a**, 570 (1962); Z. Nat.forsch. **17a**, 651 (1962).
[19] E. Simanek and K. A. Müller, J. Phys. Chem. Solids **31**, 1027 (1970).
[20] T. Estle and M. De Wit, Bull. Am. Phys. Soc. **6**, 445 (1961).

 